

## Mapping submarine sand waves with multiband imaging radar

### 2. Experimental results and model comparison

J. Vogelzang

National Institute for Coastal and Marine Management, The Hague, Netherlands

G.J. Wensink<sup>1</sup> and C.J. Calkoen<sup>1</sup>

Delft Hydraulics, Marknesse, Netherlands

M.W.A. Van der Kooij<sup>2</sup>

Physics and Electronics Laboratory, The Hague, Netherlands

**Abstract.** On August 16, 1989, and on July 12, 1991, experiments were performed to study the mapping of submarine sand waves with the airborne imaging radar, a polarimetric (and, in 1991, interferometric) airborne P, L, and C band synthetic aperture radar system. The experiments took place in an area 30 km off the coast of the Netherlands, where the bottom topography is dominated by sand waves with a height between 2 and 6 m and a crest-to-crest distance of about 400 m at an average depth of 22 m. Ground measurements were recorded on a nearby platform and on a ship in the test area, which also acted as a position fix. On August 16, 1989, the wind was 5 m/s directed toward the northeast, while the surface current velocity was around 0.5 m/s directed toward the southwest. One overflight was made, with the flight direction parallel to the sand wave crests and the radar looking upwind. At P band, the sand waves are clearly visible as dark bands, as predicted by theory, while at L band the sand waves show up as sawtooth-shaped modulations. On July 12, 1991, wind and surface current had the same (opposite) directions as in 1989, though the wind was much higher (10 m/s). Three flights were made, with the radar pointing upwind, cross wind, and downwind. The upwind and downwind images are very similar. Despite the high wind speed, the sand waves are clearly visible as sawtooth-shaped modulations at P band and vaguely visible at L band. At C band, only wind streaks can be seen. All cross wind images show the sand waves as dark bands, now with the highest modulations at C band. The wind streaks that dominated the upwind and downwind images at C band are much less pronounced in the cross wind images. The images are compared with predictions from a new model of the imaging mechanism which includes contribution to the radar cross section of waves moving both from and to the radar. Wave blocking or wave reflection is treated in an approximate manner. For the radar looking upwind or downwind, the predicted modulations at P and L band agree well with the observations, while those at C band are too high. For the radar looking cross wind, the model severely underestimates the modulations. It is questioned whether a local relaxation source term can describe such a situation. The interferogram shows some structure caused by bottom-induced surface current variations.

### 1. Introduction

The first observations of submarine sand waves with imaging radar were made in 1969 by De Loor *c.s.* [De Loor and Brunsveld van Hulst, 1978; De Loor, 1981].

These experiments and subsequent ones in the mid 1970s were performed with side-looking airborne radar (SLAR). The radar systems were neither geometrically nor radiometrically calibrated, so only qualitative comparisons with predictions from models for the imaging mechanism [e.g., Alpers and Hennings, 1984] were possible.

In 1988 an experiment was performed with the Dutch digital SLAR (DDSLAR), a geometrically and radiometrically calibrated X band system. The experiment took place in a sand wave area 30 km off the coast of the Netherlands [Vogelzang *et al.*, 1992]. Since the DDSLAR was originally developed for land use, the radiometric calibration was switched off during the experiment in order to increase its sensitivity. The resulting images were still

<sup>1</sup>Now at Advisory and Research Group on Geo Observation Systems and Services, Marknesse, Netherlands.

<sup>2</sup>Now at Atlantis Scientific Systems Group Inc., Ottawa, Ontario, Canada.

geometrically calibrated, though very noisy. By comparing the images with a digitized depth map, it was concluded that the steep slopes of the sand waves show up as light or dark bands, depending on the current direction, as predicted by models for the imaging mechanism [Alpers and Hennings, 1984; Vogelzang, 1989].

On August 16, 1989, and July 12, 1991, the same area was studied with the polarimetric (and in 1991 interferometric) airborne imaging radar (AIR) of the National Aeronautics and Space Administration, Jet Propulsion Laboratory (NASA-JPL). The AIR is a synthetic aperture radar (SAR) which operates at P, L, and C band.

The AIR experiments have already been presented and discussed extensively in reports [Vogelzang *et al.*, 1991; Calkoen and Van der Kooij, 1993]. Comparison with model predictions was done by Hennings *et al.* [1994] and Van der Kooij *et al.* [1995]. Nevertheless, the authors believe that the data set gathered during the AIR campaigns deserves a more complete presentation in the open literature, since it contains some new, highly interesting features. During both experiments, wind and current had opposite directions, the wind coming from the southwest and the current heading toward the southwest, almost perpendicular to the sand wave crests. In the 1989 experiment the conditions were calm (wind speed about 5 m/s) with surface current velocity between 0.4 and 0.5 m/s. Only images with the flight direction parallel to the sand wave crests and the radar looking upwind were made. The 1991 experiment took place under rough conditions (wind speed 10 - 12 m/s) with slightly higher surface current velocity (0.5 - 0.6 m/s). Besides images with the flight direction parallel to the sand wave crests (radar look direction both upwind and downwind), images with the flight direction perpendicular to the crests (radar looking cross wind) were also made.

The P band image of 1989 shows the sand waves clearly as narrow dark bands. The modulations at L band are weaker. At C band, no clear sand wave signals are found, except at low incidence angles. The upwind images of 1991 show a similar behavior: despite the high wind speed the sand waves are visible at P band and very weakly visible at L band, while the C band image shows only wind streaks. The downwind images of 1991 show the sand waves only weakly at P band. The magnitude of the modulations and their variation with radar frequency can be understood well from existing theory [Hennings *et al.*, 1994; Van der Kooij *et al.*, 1995]. In the cross wind images, the sand waves are visible as dark bands, clearly at C band, less clear at L band, and weakly at P band. The bands are broader than those in the P band image of 1989. The wind streaks are much less pronounced than for the upwind and downwind images.

On closer inspection, the shape of the modulations in the L band image of 1989 and in the upwind and downwind P and L band images of 1991 differs from what has been observed before. Instead of a modulation pattern consisting of dips over the steep slopes as predicted by existing models for the imaging mechanism, these images show a sawtooth-shaped modulation pattern, as noticed first by one of the authors (MVdK).

In a companion paper, Vogelzang [this issue] extends existing theory into a new model. The model includes contributions to the radar cross section of waves moving both from and to the radar. By assuming a Pierson-Mos-

kowitz radial equilibrium wave height spectrum with an angular distribution as given by Hasselmann *et al.* [1980] and by assuming an angular dependency of the relaxation rate as proposed by Lyzenga [1991], these modulations can be explained, at least qualitatively. Wave blocking or wave reflection is included in an approximate, as simple as possible manner. Due to the algorithm employed, the value of the wave height spectrum density at blocking wavenumbers must be given explicitly. This value only affects the magnitude of the resulting modulations at P band; the shape of the modulation pattern is less affected. See Vogelzang [this issue] for more details. It should be noted that the model is restricted to a (quasi) one-dimensional bottom as considered here.

Section 2 contains a brief description of the test area, the AIR, and the results of the experiments. In section 3 the results are discussed and compared with model predictions. It will be shown that the bottom-induced modulations observed in the AIR images can be understood when the radar look direction is parallel or antiparallel to the current direction. For P and L bands the agreement between theory and experiment is satisfactory; for C band the model predictions are too high. Better agreement could be obtained by tuning the relaxation rate in the downwind direction. When the radar look direction is perpendicular to the current, the predicted modulations are much too low. It is questioned whether a model based on a local relaxation source term can describe bottom-induced modulations in such cases. The paper ends with the conclusions in section 4.

## 2. Experiments and Results

### 2.1. Test Area and Flow Model

The test area is located in the Southern Bight of the North Sea, 30 km off the coast of the Netherlands near the town of Noordwijk (Figure 1). The area is relatively close to the Measuring Platform Noordwijk (MPN), a fixed platform which is part of the North Sea Monitoring Network. On MPN, data on wind, temperature, and waves are collected on a routine base.

The bottom topography in the test area is dominated by sand waves with a height between 2 and 6 m and a crest-to-crest distance of typically 400 m at an averaged depth of 22 m. The crest lines are oriented northwest-southeast, perpendicular to the coastline and the dominating current direction. A detailed bathymetric map of the area on a 5 m x 5 m grid was made in 1991 with multibeam echo sounders [Vogelzang, 1993]. The sand waves have an asymmetric profile, resembling sawtooths rather than sines, with a steep slope of typically 40 m length directed toward the northeast [Van der Kooij *et al.*, 1995].

For this test area a quasi-three-dimensional flow model is available. It consists of a two-dimensional model for the depth-averaged current velocity in which the shallow water equations are solved numerically [Leendertse, 1967; Stelling, 1984]. It receives its boundary conditions from similar models on a larger scale. Once the depth-averaged current velocity is known, the current profile is reconstructed following the approach of Davies [1987]. As an extension, the influence of the wind on the surface current has been included [Zitman, 1992]. The model and some of its simplifications have been verified by Vogelzang *et al.* [1991] and Calkoen and Van der Kooij [1993].



Figure 1. Location of the test area.

## 2.2. Airborne Imaging Radar

The AIR is a polarimetric (and, in 1991, interferometric) SAR of NASA-JPL. The AIR operates at three radar bands: P, L, and C band. It is carried by a modified DC-8 passenger jet. Its most important specifications are listed in Table 1. The specifications of the AIR differ slightly for the two experiments due to an upgrade of the system in between.

## 2.3. Results of the 1989 Experiment

On August 16, 1989, one overflight was made with the AIR. Flight direction and acquisition time are given in Table 2. During the overflight, the *Octans*, a ship of Rijkswaterstaat, was anchored near the center of the test area at position  $52^{\circ}23'03.12''\text{N}$ ,  $4^{\circ}02'02.78''\text{E}$ . The ship's position was recorded using radio positioning (the so-called HYPERFIX system) with an accuracy of about 1.5 m, in order to use the image of the ship as a position fix. Current profiles were measured from the ship, using an Ott current meter and an Elmar direction meter. From the profiles the surface current velocity during the AIR overpass was estimated. This estimate agrees well with the surface current velocity calculated with the quasi-three-dimensional flow model. Wind, wave, and temperature data were recorded on MPN as 10-min averages. The most important hydro-meteo parameters are listed in Table 2. Note that the wind direction indicates the direction from which the wind is blowing, whereas the current direction gives the direction into which the current is flowing. All directions are measured clockwise from the north.

Table 1. AIR Specifications

	P band	L band	C band
Frequency, MHz	428-450	1238-1260	5288-5310
Center frequency	438.75	1248.75	5298.75
Wavelength, cm	68.38	24.02	5.662
Look angle range	$21.3^{\circ}$ - $61.7^{\circ}$	$21.3^{\circ}$ - $61.7^{\circ}$	$21.3^{\circ}$ - $61.7^{\circ}$
Azimuth pixel size	12.10 m	12.10 m	12.10 m
Slant range pixel size	6.67 m	6.67 m	6.67 m
Image size 1989*	1024×750	1024×750	1024×750
Image size 1991*	1024×1279	1024×1279	1024×1279

\*Range x azimuth

Table 2. Flight and Hydro-meteo Parameters for the 1989 experiment

Parameter	Value
Acquisition time, UT	080707
Flight direction	$121^{\circ}$
Wind speed at 10 m	5.0 m/s
Wind direction	$211^{\circ}$
Surface current velocity at troughs	0.5 m/s
Surface current direction	$210^{\circ}$
Peak wavelength	48 m
Significant wave height	57 cm
Air temperature	$19.1^{\circ}\text{C}$
Water temperature	$18.7^{\circ}\text{C}$

The conditions were favorable for mapping bottom topography: the wind was around 5 m/s from the southwest, while the surface current velocity, directed toward the southwest, ranged from about 0.7 m/s above the sand wave crests (depth 19 m) to about 0.5 m/s above the troughs (depth 25 m). The error in the current velocity measurements is 10% in magnitude and  $5^{\circ}$  in direction. Note that wind and current had opposite directions.

The AIR 1989 P and L band images at vertical (VV) polarization are shown in Figure 2. The images are converted to ground range with a pixel size of 10 m in both directions. The dependency of the radar cross section on the incidence angle has been removed in Figure 2, in order to make the modulations more clearly visible.

Figure 3 shows the modulation patterns for the P and L band VV polarized images of 1989. In order to reduce speckle, the curves in Figure 3 are an average over 101 lines. Also, the corresponding bottom profile is shown in Figure 3. The solid curve gives the depth along the central image line; the dotted curves give the depth along the extreme outer lines.

At P band the steep slopes of the sand waves show up as narrow dark bands, as can be seen in Figures 3 and 2. Both position and magnitude of the modulations in this image are described very well by relaxation models [Vogelzang et al., 1991; Hennings et al., 1994; Van der Kooij et al., 1995]. The sand waves are also visible in the L band image, but not as clear as in P band. A closer inspection of the L band images reveals a peculiar phenomenon: the sand waves express themselves not as dark bands as expected from theory but as sawtooth-shaped modulations (see Figure 3). This point will be returned to later. The C band image shows little structure (no result shown). Some faint sand wave modulations can be discerned at low incidence angles.

There is no sign that the modulations at P and L bands depend on the polarization [Vogelzang et al., 1991]. As a consequence, VV polarization is to be preferred, since at this polarization the backscatter from the sea surface is highest, yielding the best signal-to-noise ratio.

## 2.4. Results of the 1991 Experiment

On July 12, 1991, the AIR made three flights over the test area. Flight directions and acquisition times are given in Table 3. The first flight was made with the AIR in

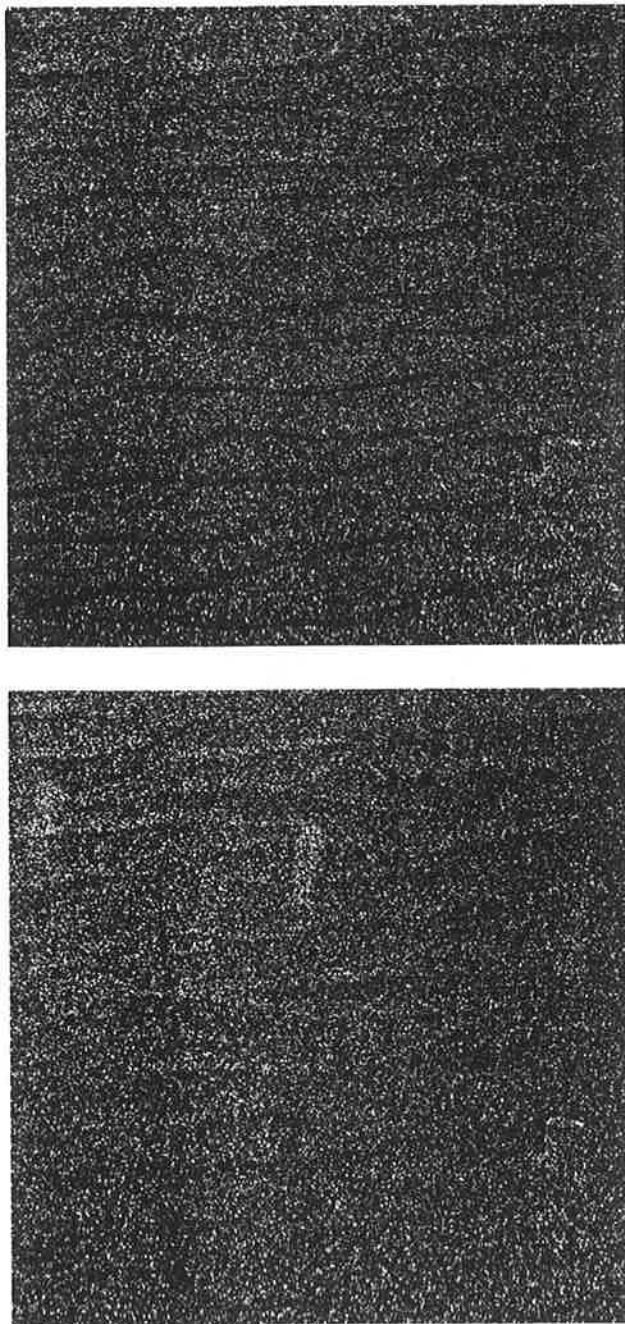


Figure 2. AIR (top) P band and (bottom) L band images at VV polarization, recorded on August 16, 1989. The horizontal structures are caused by sand waves.

interferometric mode; the two other flights were made in normal SAR mode. Microwave measurements were also performed with a helicopter-borne multipolarization, multifrequency scatterometer (HELISCAT) operated by the University of Hamburg, and a Dutch experimental airborne C band SAR (PHARS). See Vogelzang [1993] for more details.

As during the 1989 experiment, the *Octans* was anchored in the test area to measure the current velocity profile and to act as a position fix. Its position was measured with differential global positioning system (DGPS) to a precision of 2 m. Unfortunately, the system failed during the

experiment. At 0850 UT, just before the first overflight, the position of the *Octans* was 52.369572°N, 4.001369°E, while at 0951 UT, right after the last overflight, its position was 52.369328°N, 4.002614°E; a difference of 90 m. Due to the rough weather conditions, only three current profiles could be measured between 0819 and 1003 UT. The profiles are heavily disturbed by the ship's movements. Therefore the quasi-three-dimensional flow model was used to hindcast the surface current velocity. The wind measured at MPN was coming from the southwest and increased from 10 m/s to 12 m/s during the experiment. The significant wave height was estimated by visual inspection on the *Octans*. The most important hydro-meteo parameters are given in Table 3.

Figures 4 and 5 show the two best images obtained in during the AIR 1991 experiment. The images are converted to ground range with a pixel size of 10 m in both

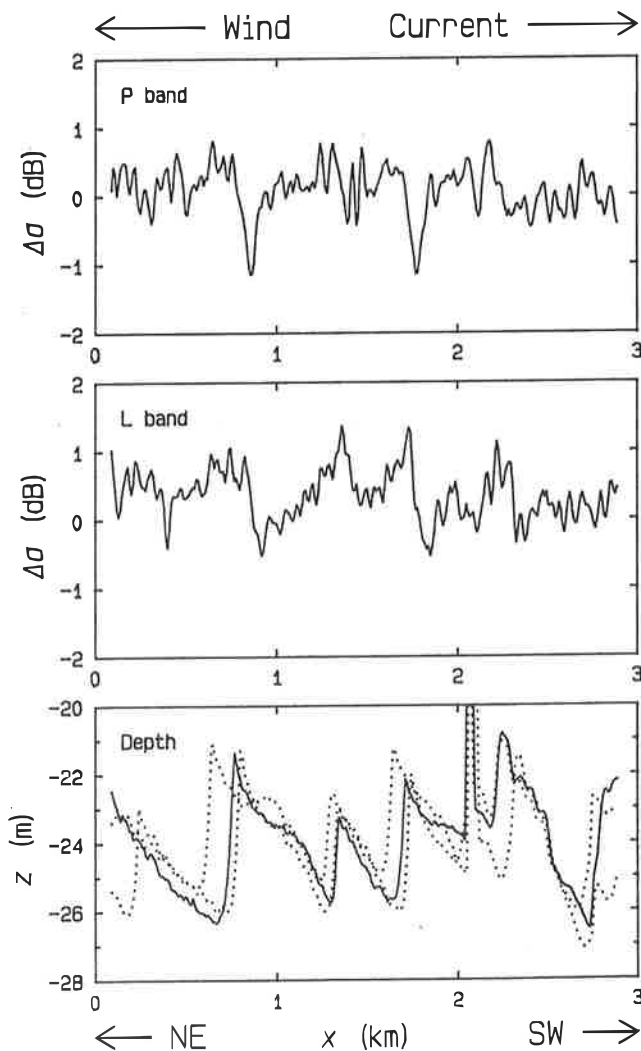


Figure 3. Depth profiles (bottom panel) and modulation in the radar cross section at L band (middle panel) and P band (top panel) observed during the AIR 1989 experiment. The modulations are averaged over 101 image lines. The solid depth profile is along the central line; the dotted ones are along the outer lines. The directions of northeast (NE) and southwest (SW), as well as those of wind and current are indicated.

**Table 3.** Flight and Hydro-meteo Parameters for the 1991 experiment

	1991-A	1991-B	1991-C
Acquisition time, UT	0901	0916	0932
Flight direction	121°	211°	301°
Wind speed at 10 m, m/s	10	11	12
Wind direction	230°	230°	230°
Surface current velocity, m/s	0.55	0.55	0.55
Surface current direction	210°	210°	210°
Significant wave height, m	2	2	2

directions. The variation of the radar cross section with incidence angle has been removed by hand. In order to reduce speckle, a 3 by 3 median filter has been applied. The conditions were much less favorable for mapping bottom topography than during the 1989 experiment due to the high wind speed, though the surface current velocity was slightly higher, about 0.55 m/s above the troughs and about 0.7 m/s above the crests. Therefore it was a surprise that the sand waves are visible in some of the AIR images.

The first flight (track 1991-A) was performed with the radar looking upwind and the flight direction parallel to the sand wave crests (same geometry as in the 1989 experiment). At P band the sand waves are visible as sawtooth-shaped modulations like in the L band images of 1989, with the strongest modulations at VV polarization. This image is shown in Figure 4. Besides sand wave modulations the images also contain wind streaks perpendicular to

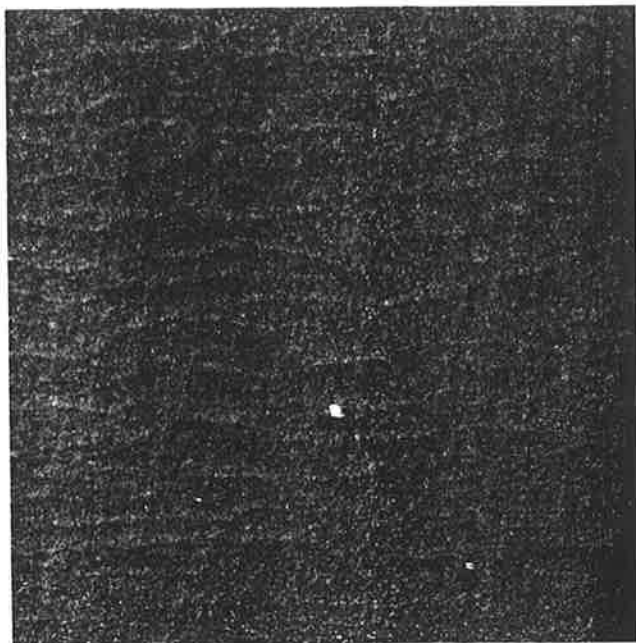


**Figure 4.** The AIR 1991-A image of July 12, 1991, for P band at VV polarization. The horizontal bands are caused by sand waves; the vertical striping is due to wind streaks. The two bright spots, one below the center (*Octans*) and one at lower right, are ships.

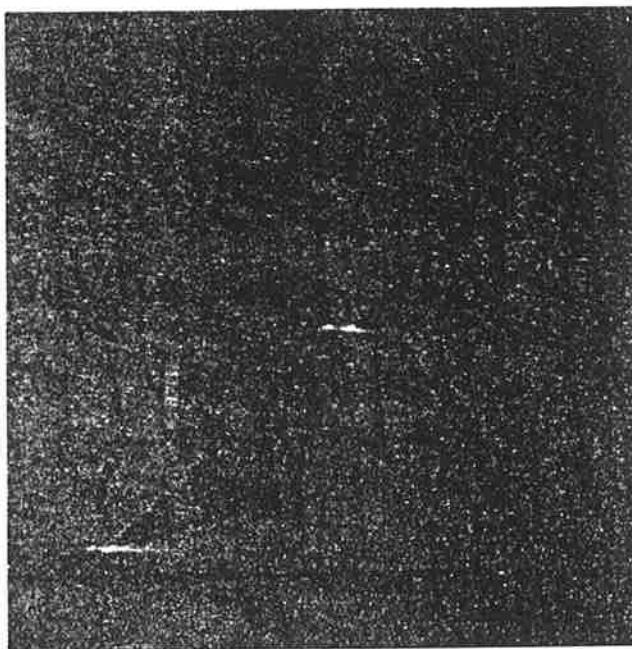


**Figure 5.** The AIR 1991-B image for C band at HH polarization. The sand waves are now vertical; the wind streaks horizontal. The two bright elongated spots, one in the center (*Octans*) and one at lower left, are ships.

the sand wave crests. At L band the sand wave modulations are very vague, while at C band the image is dominated by wind streaks (no results shown). The modulation depth in the radar cross section decreases with decreasing radar frequency, as described by the model of Van der Kooij *et al.* [1995].

The images of the second run, track 1991-B, were made with the radar range direction pointing cross wind and the flight direction perpendicular to the sand wave crests. Surprisingly, the sand waves are faintly visible as dark bands in these images. The strongest modulations are found at C band and HH polarization. This image is shown in Figure 5. In contrast with the images obtained in run 1991-A, the modulation depth increases slightly with decreasing radar frequency. The wind streaks, which were dominant for upwind radar range direction, are much weaker, but still visible.

The images of the third run, track 1991-C, were made with the radar range direction pointing downwind and the flight direction parallel to the sand wave crests. The images are similar to those obtained in run 1991-A, though the modulations are weaker. The sand waves are visible as sawtooth-shaped modulations at P band and hardly visible at L band, while the C band image is dominated by wind streaks (no results shown).

The modulation pattern, averaged over 101 images lines, is shown in Figure 6 for the VV polarized P and L band images of 1991 run A, together with the depth profiles along the central line (solid curve) and along the outer lines (dotted curves). Note that the relative positioning between depth map and radar images may have an error up to about 100 m, due to the fact that the ship's position was not measured during the overflights.

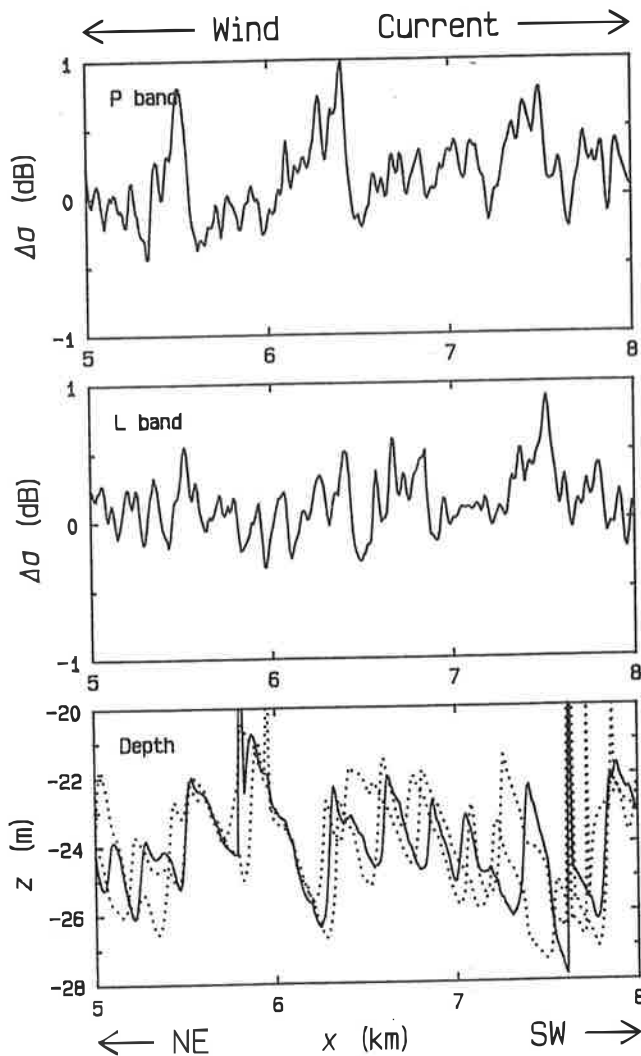


Figure 6. As in Figure 3, for the AIR 1991-A experiment.

The average modulation depths in dB, i.e., the averaged differences between minimum and maximum radar cross section, are given in Table 4. Negative modulation depths indicate dark band modulations, while positive modulation depths indicate sawtooth-shaped modulations.

Run 1991-A was made with the AIR L band in interferometric mode. The resulting interferogram is a noisy image which shows some faint expressions of the sand waves and some artifacts of unknown origin (no results shown). By averaging over a number of lines in the interferogram, the surface current modulation was estimated to

Table 4. Observed Modulation Depths

Run	$P_{VV}$	$P_{HH}$	$L_{VV}$	$L_{HH}$	$C_{VV}$	$C_{HH}$
1989	-2.0	-2.0	+1.0	+1.0	0	0
1991-A	+1.0	+0.9	+0.5	+0.5	0	0
1991-B	-0.5	-0.6	-0.6	-0.6	-0.7	-0.8
1991-C	+0.5	+0.5	0	0	0	0

Values are given in decibels.

be  $0.10 \text{ m/s} \pm 0.05 \text{ m/s}$ , which corresponds to the expected change of the current velocity over the steep slopes of the sand waves. The phase noise is approximately  $0.15 \text{ m/s}$ . Due to the high wind speed, the decorrelation time of the waves is of the same order of magnitude as the time interval between the passes of front and aft antenna (0.05 s). This caused a significant decorrelation of the radar backscatter and thus phase noise in the interferogram.

### 3. Comparison With Model Predictions

#### 3.1. The 1989 Experiment

Figure 7 shows the modulation in the radar cross section,  $\Delta\sigma$ , as a function of position  $x$  for P, L, and C bands. The curves were obtained for two adjacent sand waves with the model developed by Vogelzang [this issue]. The sand waves are schematized as sawtooth-shaped structures with the depth varying between 19 m at the crests to 25 m at the troughs. The total sand wave length is 400 m; the steep slope length is 40 m. The  $x$  coordinate is directed toward the southwest. The current velocity above the troughs is  $0.5 \text{ m/s}$  in the positive  $x$  direction, and the wind

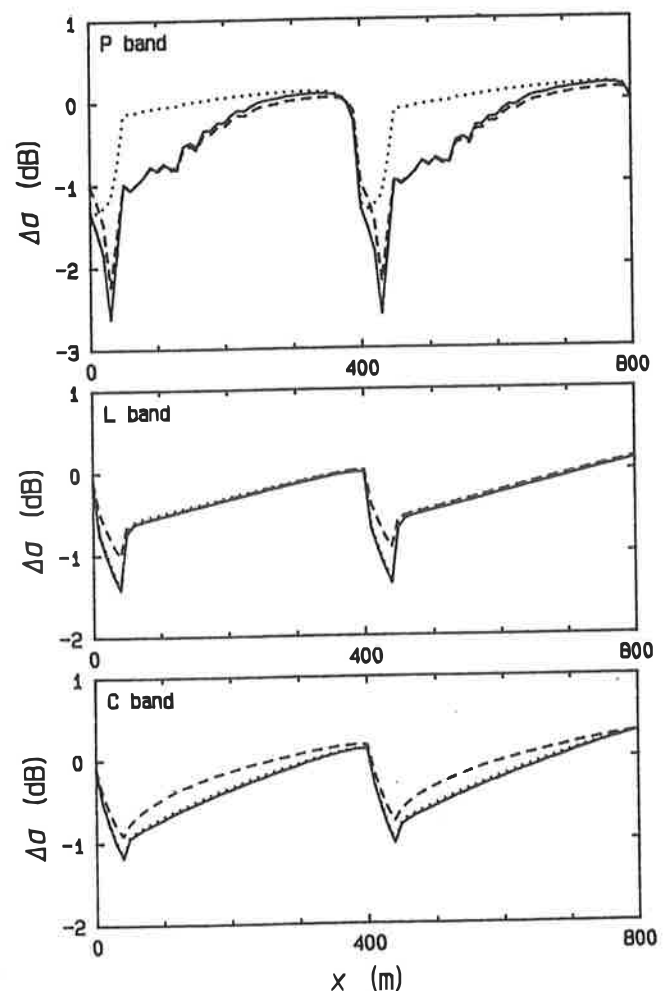


Figure 7. Predicted modulations for the AIR 1989 images with the upwind relaxation rate of Hughes [1978] (solid curves) and that of Hsiao and Shemdin [1983] (dashed curves). The dotted curve is obtained by setting the wave spectrum at blocking equal to its equilibrium value.

speed is 5.0 m/s in the negative  $x$  direction. The radar cross section,  $\sigma$ , is calculated with the integral equation scattering model of *Holliday et al.* [1986]. The solid curves correspond to the standard calculation defined by *Vogelzang* [this issue]. For the equilibrium wave height spectrum a Pierson-Moskowitz form was chosen with the angular distribution of *Hasselmann et al.* [1980]. The peak position parameter and the strength parameter were adjusted to yield the peak wavelength and significant wave height in Table 2. The wave spectrum was set equal to zero at blocking. The source term is given by a linear relaxation form, with the parameterization of *Hughes* [1978] for the upwind relaxation rate and the prescription of *Lyzena* [1991] for its angular behavior.

The predicted modulations in  $\sigma$  consist of two components: one originating from waves moving away from the radar and one from waves moving toward the radar (in a frame of reference at rest relative to the water). When the wind is parallel or antiparallel to the radar look direction, the resulting modulations depend on the angular distribution and the equilibrium wave height spectrum as well as the angular behavior of the relaxation rate.

With the choices mentioned above, the model predicts negative modulations of about 2.5 dB right above the steep sand wave slope for P band, in agreement with the observations. Since the equilibrium wave height spectrum of waves contributing to the P band cross section is peaked into the wind direction, the modulations originate from waves moving with the wind. The P band results are affected by numerical noise beyond the steep slopes, due to the fact that waves contributing to  $\sigma$  may encounter blocking conditions. At blocking, the wave height spectral density is set equal to zero, corresponding to total dissipation at blocking. Wave reflection can be included approximately by setting the wave height spectral density at blocking equal to its equilibrium value (dotted curves in Figure 7). This results in more regular negative modulations of about 1.5 dB. The magnitude of the modulation depth can be increased or decreased by 0.5 dB using another parameterization for the upwind relaxation rate. The dashed curves give the results using the parameterization of *Hsiao and Shemdin* [1983].

For L band the angular distribution of waves contributing to  $\sigma$  is more isotropic. Therefore both waves moving with the wind and waves moving against it contribute to  $\sigma$ . As a consequence,  $\Delta\sigma$  consists of two components: a dip pattern above the steep slope caused by waves moving with the wind and a sawtooth pattern caused by waves moving against the wind. The latter waves have zero or small relaxation rate and are advection dominated [*Vogelzang*, 1989]. They have maximum hydrodynamic modulation which varies little with wavenumber and which is proportional to the surface current itself rather than its gradient. The modulation depth is 1.5 dB. The contribution of the dip pattern can be decreased by choosing the parameterization of the upwind relaxation rate of *Hsiao and Shemdin* [1983], yielding only a sawtooth pattern with a modulation depth of 1 dB.

For C band the model results are very similar to those at L band, except that the contribution of the dip pattern is lower. The predicted modulation depth at C band is too high. This can be repaired by increasing the downwind

relaxation rate from 0 to a value near  $0.02 \text{ s}^{-1}$ . The downwind waves then are still advection dominated but will have smaller hydrodynamic modulation.

One expects a transition zone where both contributions to  $\sigma$  are equally important. This seems to be the case in the P band 1989 image for high incidence angles. Here  $\sigma$  originates from waves with high wavenumber (compared to low incidence angles), the angular distribution of which is more isotropic. Therefore the contribution of waves moving against the wind becomes more important.

The model results are obtained with an incidence angle of  $23^\circ$ . The scattering model of *Holliday et al.* [1986] is restricted to these small incidence angles. However, first-order Bragg scattering performs equally well. At P band, contributions of waves longer than the Bragg waves are not important. At L and, notably, C band these contributions are important, but here the modulations are dominated by waves moving against the wind which have zero or small relaxation rate. Their hydrodynamic modulation varies little with wavenumber, so first-order Bragg scattering can be applied. *Van der Kooij et al.* [1995] show that the modulation depth calculated with first-order Bragg scattering varies little with incidence angle. The agreement

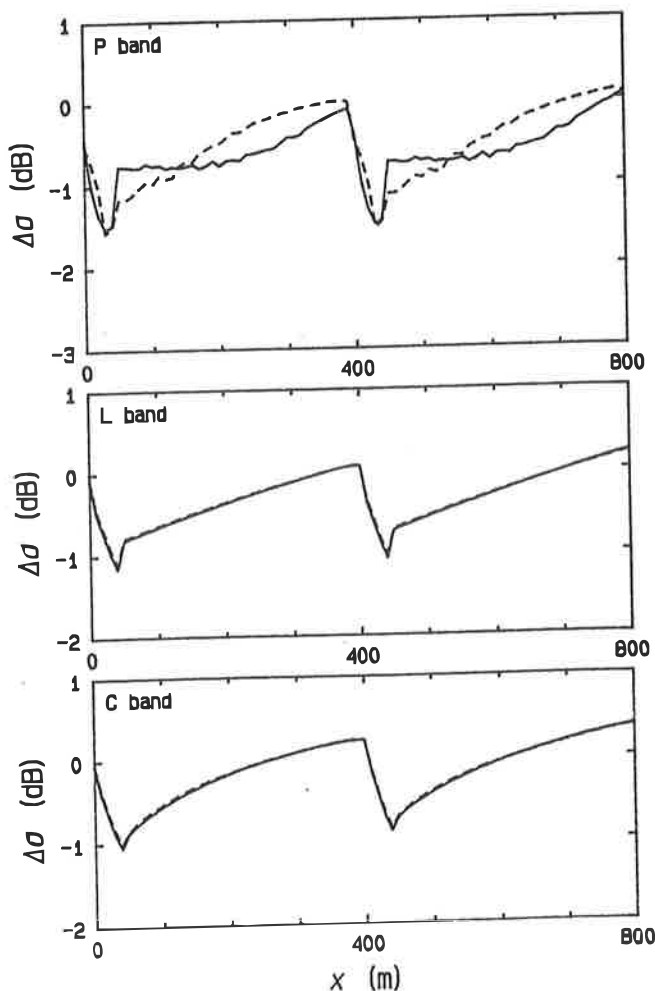


Figure 8. Predicted modulations for the AIR 1991-A images with a surface current velocity above the troughs of 0.55 m/s (solid curves) and 0.50 m/s (dashed curves).

between theory and experiment is good for the AIR 1989 images, except at C band where the predicted modulations are too high.

### 3.2. The 1991 Experiment

Figure 8 shows the model results for the AIR 1991-A images, with a current velocity above the crests of 0.55 m/s (solid curves) or 0.50 m/s (dashed curves), a wind speed of 10 m/s, and all other parameters remaining the same. At P band the modulation depth is about 1 dB. The shape of the modulation is very sensitive to the value of the current velocity, due to the fact that this determines whether waves contributing to  $\sigma$  may be blocked or not. The best agreement with the experimental results is obtained for a current velocity of 0.50 m/s. Since the current velocity during the AIR 1991 experiment was estimated from model hindcasts, a disagreement of 0.05 m/s is well within the expected precision.

For L and C bands the modulation depth is about 1 dB, since  $\Delta\sigma$  is dominated by waves moving against the wind which have zero or small relaxation rate (see previous section). The modulation depth can be reduced also here by tuning the downwind relaxation rate.

Figure 9 shows the results for the 1991-B conditions. The solid curves were obtained with the standard input and show a broad dip pattern above the steep slope. Note that the predicted modulations in  $\sigma$  are very small: the modulation depth is 0.1 dB or less, whereas the observed values lie between 0.5 dB and 0.8 dB. This is caused by the fact that the waves contributing to  $\sigma$  have very small hydrodynamic modulation. They move almost perpendicular to the current variations and therefore feel little effect of it. The dashed curve at C band is obtained with a  $\cos^{16}(\phi/2)$  angular behavior of the relaxation rate, reducing the relaxation rate at  $\phi = 90^\circ$  by a factor of 128. The modulations become stronger but are still much weaker than observed. Moreover, the modulations get a sawtooth shape, due to the low relaxation rate of waves contributing to  $\sigma$ . The model is not able to explain the modulations observed in the AIR 1991-B images. This point will be returned to in the next section.

The model predictions for the AIR 1991-C images resemble strongly those for the AIR 1991-A images in Figure 8 (no results shown). The only difference is reduced strength of the dip pattern for P band, due to the higher wind speed. The results for L and C band are almost the same. The weaker modulations observed in the 1991-C image compared to those in the 1991-A image are most likely due to an increase in wind speed. Note that the model yields the same results for radar azimuth angles of  $0^\circ$  and  $180^\circ$  due to the symmetry in the scattering model.

### 3.3. Discussion

From the results presented above and those given by Vogelzang [this issue], the following general picture emerges for the mapping of sand waves with imaging radar:

The modulations in  $\sigma$  originate from two contributions: one from waves moving away from the radar (relative to a reference frame moving with the water) and one from waves moving toward the radar. The shape of the modu-

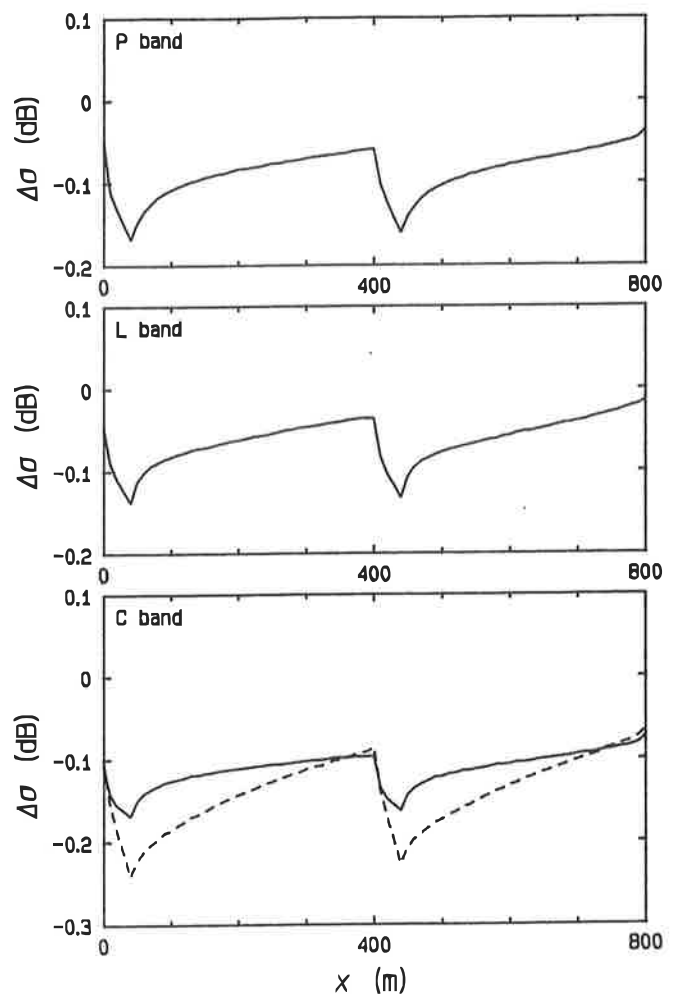


Figure 9. Predicted modulations for the AIR 1991-B images with a angular behavior of the relaxation rate of  $\cos^2(\phi/2)$  (solid curves) and  $\cos^{16}(\phi/2)$  (dashed curve).

lations depends critically on the angular distribution of the equilibrium wave height spectrum and the angular behavior of the relaxation rate.

When the radar look direction is parallel or antiparallel to the current direction within about  $30^\circ$ , the best results are obtained with the angular distribution of Hasselmann *et al.* [1980] and with the angular relaxation rate of Lyzenga [1991]. The angular distribution is peaked in the wind direction but becomes isotropic at high wind speeds and high wavenumbers. The relaxation rate becomes zero for waves moving against the wind.

When the wind is also parallel or antiparallel to the current direction, the shape of the modulations depends on wind speed. For P band at wind speeds of 5 m/s or less and for L band at wind speeds of 2.5 m/s or less, the equilibrium wave spectrum of waves contributing to  $\sigma$  is peaked into the wind direction. Therefore only the upwind part of the wave spectrum contributes. These waves have a relaxation rate much larger than  $0.02 \text{ s}^{-1}$ , and  $\Delta\sigma$  is proportional to the current gradient and hence to the bottom slope. This accounts for the dip pattern in the AIR 1989 P band image.

For P band at wind speeds higher than about 5 m/s, for

L band at wind speeds higher than about 2.5 m/s, and for C band at all wind speeds, the angular distribution of waves contributing to  $\sigma$  becomes isotropic. Waves moving against the wind contribute as much to  $\sigma$  as waves moving with the wind. However, waves moving against the wind have zero or small relaxation rate. These waves are advection dominated and exhibit maximum hydrodynamic modulation [Vogelzang, 1989]. The modulations in  $\sigma$  are dominated by these waves, accounting for the sawtooth-shaped modulations observed in the AIR 1989 and 1991 images.

First-order Bragg scattering performs well for all radar bands when the wind is parallel or antiparallel to the current direction. This is either because the radar wavelength is large, so waves larger than the Bragg waves have little influence, or because the hydrodynamic modulations depend little on wavenumber.

When the wind speed is more perpendicular to the current direction, both waves moving from and to the radar contribute to  $\sigma$ . Generally, the waves have a relaxation rate larger than  $0.02 \text{ s}^{-1}$ , and the sand waves will show up as bright or dark bands. Depending on the exact magnitude of the relaxation rate, advective effects may broaden the sand wave signatures, as observed with ERS 1 [Vogelzang et al., 1994]. First-order Bragg performs well at P and L bands, but at C band the effect of waves longer than the Bragg waves must be taken into account to explain the magnitude of bottom induced modulations.

When the radar look direction is perpendicular to the current direction, as in the 1991-B AIR images, waves contributing to  $\sigma$  move (almost) perpendicular to the current variations. The hydrodynamic modulation of these waves is very weak. It is zero for wave moving exactly perpendicular to the current variations. Integral equation scattering models predict too low modulations, while first-order Bragg scattering predicts no modulations at all. Nevertheless, the sand waves are visible. A similar observation at X band was reported by Vogelzang et al. [1992].

It is questionable whether a model with a local relaxation source term can account for the 1991-B observations. The waves contributing to  $\sigma$  in this case move almost perpendicular to the current variations and therefore feel little effect of it. An explanation might be given by the following considerations. Only waves moving with the wind receive their energy directly from the wind. Waves moving in other directions obtain their energy from wind-driven waves via nonlinear wave-wave interactions. When the wind-driven waves are modulated by current variations, the energy transport is affected and the other waves will follow quickly, because energy transport via nonlinear wave-wave interactions is very efficient. It is most likely that waves moving perpendicular to a varying current still feel sizable effects of it, due to such a mechanism. The results of the AIR 1991-B experiment indicate that the wave height spectral density of waves moving perpendicular to the wind is restored quickly to its equilibrium value. The wave height spectral density of waves moving against the wind, which is also affected directly by the current variations, needs much more time to reach equilibrium again. Note that a local source term is not able to account for such a mechanism.

The mechanism outlined above is corroborated by the fact that the wind streaks, which dominate the 1991-A and 1991-C images, are also visible in the 1991-B images. Apparently, wave height variations in the wind direction spread also to other directions.

#### 4. Conclusions

In this paper we presented the results of two experiments with the AIR, a polarimetric and interferometric P, L, and C band airborne SAR, in a sand wave area in the North Sea. The sand waves have an asymmetric profile, with a steep slope oriented toward the northeast. During both experiments, the current direction was perpendicular to the sand wave crests, while wind and current had opposite directions. The AIR images contain two striking features. First, the sand waves were sometimes visible even at high wind speed (10-12 m/s). Second, two types of modulations were observed: dip shaped and sawtooth shaped.

When the radar look direction is perpendicular to the sand wave crests, the steep slopes of the sand waves show up as narrow dark bands for P band at low wind speed (1989 experiment). This is explained by the fact that the angular distribution of waves contributing to the radar cross section is peaked into the wind direction. For higher wind speed and/or for higher radar wavenumbers (L band of 1989, P and L band of 1991-A, and P band of 1991-C), the sand waves cause sawtooth-shaped modulations which have not been reported before. These modulations are explained by the fact that the wave height spectrum of waves contributing to the radar cross section becomes isotropic. The modulations are dominated by waves moving against the wind, which have zero or very small relaxation rate.

The decrease of the observed modulations with increasing wind speed and increasing radar wavenumber has already been explained. The shape of the observed modulations can be explained by extending existing theory, though the resulting model predicts too high modulations for C band and for L band at high wind speeds. This may be repaired by tuning the downwind relaxation rate.

When the radar look direction is parallel to the sand wave crests (and perpendicular to the current direction) the sand waves are visible as dark bands (P, L, and C band of 1991-B). Here the modulations increase slightly with increasing radar wavenumber. These modulations cannot be explained by the models. It is likely that a correct description requires a nonlocal source term.

The modulations in the radar cross section do not depend significantly on polarization. Since the strongest modulations occur at low wind speeds, when the radar return from the sea surface is low, and since VV polarization has the highest signal-to-noise ratio, this polarization is to be preferred for mapping sea bottom topography and other phenomena caused by wave-current interaction (internal waves, swell, etc.). C band images are much more sensitive to wind streaks than L or P band images. Generally, the highest modulations are observed at P band. Therefore this band is best suited for mapping bottom topography.

The results of the AIR experiments show that, though some progress has been made, even the mapping of relatively simple bottom structures is still not understood completely. Precise in situ measurements of the short wave spectrum and the relaxation rate are needed to gain more insight in the imaging mechanism and to check the assumptions made here in the shape of the angular distribution of the equilibrium wave spectrum and the angular behavior of the relaxation rate.

**Acknowledgments.** The acquisition of the data during the 1989 and 1991 experiments and the interpretation of the 1989 results were financially supported by the Netherlands Remote Sensing Board (BCRS) as a part of the National Remote Sensing Programme (NRSP). The interpretation of the 1991 results was financially supported by the Commission of the European Communities as a part of the Marine Science and Technology (MAST) programme under contract MAST-0040. The authors are indebted to G. van der Burg (National Aerospace Laboratory NLR) for his assistance in preparing the AIR flights. We thank J.E. Klein and R. Carande (Jet Propulsion Laboratory) for making the data available and giving advice in interpreting the interferogram. The ground measurements were performed by the North Sea Directorate of Rijkswaterstaat. We would like to mention H.C. Peters and C. Bijleveld, who planned the ship measurements, and the captain and crew of the *Octans*, in particular T. Krijthe, who performed the current and position measurements. Finally, the authors like to thank W. Alpers, V. Wismann, and R. Romeiser (University of Hamburg, Germany), I. Hennings (GEOMAR, Germany), J.P. Matthews (School of Ocean Sciences, U.K.), and G.P. de Loor, for their interest in this work and stimulating discussions.

## References

- Alpers, W., and I. Hennings, A theory for the imaging mechanism of underwater bottom topography by real and synthetic aperture radar, *J. Geophys. Res.*, 89(C6), 10,529-10,546, 1984.
- Calkoen, C.J., and M.W.A. Van der Kooij, The mapping of sea bottom topography with polarimetric P-, L- and C-band SAR, *Rep. BCRS 93-16*, Neth. Remote Sens. Board, Delft, Netherlands, 1993.
- Davies, A.M., On extracting current profiles from vertically integrated numerical models, *Coastal Eng.*, 11, 445-477, 1987.
- De Loor, G.P., The observation of tidal patterns, currents and bathymetry with SLAR imagery of the sea, *IEEE J. Oceanic Eng.*, OE-6, 124-129, 1981.
- De Loor, G.P., and H.W. Brunsveld van Hulst, Microwave measurements over the North Sea, *Boundary Layer Meteorol.*, 13, 113-131, 1978.
- Hasselmann, D.E., M. Dunckel, and J.A. Ewing, Directional wave spectra observed during JONSWAP 1973, *J. Phys. Oceanogr.*, 10, 1264-1280, 1980.
- Hennings, I., J. Matthews, and M. Metzner, Sun glitter radiance and radar cross-section modulations of the sea bed, *J. Geophys. Res.*, 99(C8), 16,303-16,326, 1994.
- Holliday, D., G. St.-Cyr, and N.E. Woods, A radar ocean imaging model for small to moderate incidence angles, *Int. J. Remote Sens.*, 7, 1809-1834, 1986.
- Hsiao, S.V., and O.H. Shemdin, Measurements of wind velocity and pressure with a wave follower during MARSEN, *J. Geophys. Res.*, 88(C5), 9844-9849, 1983.
- Hughes, B.A., The effect of internal waves on surface wind waves, 2. Theoretical analysis, *J. Geophys. Res.*, 83(C1), 455-465, 1978.
- Leendertse, J.J., Aspects of a computational model for long-period water propagation, *Memo. RM-5294-PR*, Rand Corp., Santa Monica, Calif., 1967.
- Lyzenga, D.R., Interaction of short surface and electromagnetic waves with ocean fronts, *J. Geophys. Res.*, 96(C6), 10,765-10,772, 1991.
- Stelling, G.S., On the construction of computational methods for shallow water flow problems, Ph.D. thesis, Delft Univ. of Technol., Delft, Netherlands, 1984.
- Van der Kooij, M.W.A., J. Vogelzang, and C.J. Calkoen, A simple analytical model for the modulation of sand waves in radar imagery, *J. Geophys. Res.*, 100(C4), 7069-7082, 1995.
- Vogelzang, J., The mapping of bottom topography with imaging radar: A comparison of the hydrodynamic modulation in some existing models, *Int. J. Remote Sens.*, 10, 1503-1518, 1989.
- Vogelzang, J., Mapping of sea bottom topography in a multi-sensor approach, in *MAST Days and EUROMAR Market*, edited by M. Weydert and C. Fragakis, pp 534-549, Comm. of the Eur. Communities, Brussels, Belgium, 1993.
- Vogelzang, J., Mapping submarine sand waves with multiband imaging radar, 1, Model development and sensitivity analysis, *J. Geophys. Res.*, this issue.
- Vogelzang, J., G.J. Wensink, M.W.A. Van der Kooij, and G. Van der Burg, Sea bottom topography with P-, L- and C-band SAR, *Rep. BCRS 91-40*, Neth. Remote Sens. Board, Delft, Netherlands, 1991.
- Vogelzang, J., G.J. Wensink, G.P. De Loor, H.C. Peters, and H. Pouwels, Mapping of sea bottom topography with X-band SLAR, *Int. J. Remote Sens.*, 13, 1943-1958, 1992.
- Vogelzang, J., H. Greidanus, G.J. Wensink, and R. Van Swol, Mapping of sea bottom topography with ERS-1 C-band SAR, *Rep. BCRS 94-27*, Neth. Remote Sens. Board, Delft, Netherlands, 1994.
- Zitman, T.J., 1992, Quasi 3-dimensional current modelling based on a modified version of Davies' shapefunction approach, *Cont. Shelf Res.*, 12, 143-158, 1992.

C.J. Calkoen and G.J. Wensink, Advisory and Research Group on Geo Observation Systems and Services, P.O. Box 61, 8325 ZH Vollenhove, Netherlands. (e-mail: charles.calkoen@argoss.nl; han.wensink@argoss.nl)

M.W.A. Van der Kooij, Atlantis Scientific Systems Group Inc., 1827 Woodward Drive, Ottawa, Ontario K2C0P9, Canada. (e-mail: marco.vanderkooij@atlsci.com)

J. Vogelzang, National Institute for Coastal and Marine Management, P.O. Box 20907, 2500 EX The Hague, Netherlands (e-mail: vogelz@rikz.rws.minvenw.nl)

(Received October 12, 1995; revised May 13, 1996; accepted September 16, 1996.)

# Journal of Geophysical Research

## Information for Contributors

Original scientific contributions on the physics and chemistry of the Earth, its environments, and the solar system will be considered for publication in the *Journal of Geophysical Research*. Every part of a paper submitted for publication should convey the author's findings precisely and immediately to the reader. Authors are urged to have their papers reviewed critically by colleagues for scientific accuracy and clarity of presentation.

**Typescript.** All parts of the paper must be typed double or, preferably, triple spaced on good quality white paper 8½ by 11 inches (21.5 × 28 cm) with at least 1-inch (2.5 cm) margins at top, bottom, and sides. Erasable bond, which smudges easily, and tissue paper are not acceptable. Each page of the typescript should be numbered in the top right hand corner.

Authors are expected to supply neat, clean copy and to use correct spelling, punctuation, grammar, and syntax. Spelling and hyphenation of compound words follow the unabridged *Webster's Third New International Dictionary*. The metric system must be used throughout; use of appropriate SI units is encouraged. Following recommended style and usage expedites processing and reduces the chance of error in the typesetting.

Because text footnotes are expensive to set and distracting to the reader, they should be incorporated into the text or be eliminated completely.

The typescript should be arranged as follows: (1) title page including authors' names and affiliations, (2) abstract, (3) text, (4) reference list, (5) figure legends, and (6) tables.

**Abstract.** The abstract should in a single paragraph (250 words or fewer) state the nature of the investigation and summarize its important conclusions. Listing the contents in terms such as "this paper describes" or "the paper presents" should be avoided. Use of the passive voice often indicates that the author is merely describing the procedure rather than presenting conclusions. References should not be cited in the abstract.

The abstract should be suitable for separate publication in an abstract journal and be adequate for indexing.

When a paper is accepted for publication, the author will be asked to submit electronically an abstract and index terms for the *Geophysical Abstracts in Press* (GAP), which is published approximately 1-3 months prior to publication of the article. This abstract does not replace the abstract (described above) that is published with the article. The GAP permits authors to list accepted, in press, papers by specific subject and provides AGU members with up-to-date information in their fields. Electronic submission of abstracts ensures accuracy and streamlines production of GAP, the Earth and Space Index (EASI), and the annual print indexes. AGU asks authors to carefully select index terms when they submit their GAP abstracts to ensure that a paper is classified properly in the annual year-end subject index for each journal and to allow readers to locate papers with greater ease and precision. This new system is part of AGU's strategy to move toward electronic distribution of information.

**Mathematics.** All characters available on a standard typewriter must be typewritten in equations as well as in text. The letter l and the number 1 and the letter O and the numeral 0, which are identical on most typewriters, should be identified throughout the paper to prevent errors in typesetting. Any symbols that must be drawn by hand should be identified by a note in the margin. Authors will be charged for all corrections in galley proof for material that was handwritten in the

typescript. Allow ample space (¾ inch (2 cm) above and below) around equations so that type can be marked for the printer.

Alignment of symbols must be unambiguous. Superscripts and subscripts should clearly be in superior or inferior position. Fraction bars should extend under the entire numerator.

Barred and accented characters that are available for machine typesetting may be used. Symbols that are not available and therefore must be avoided are triple dots, any accents (other than bars) that extend over more than one character, and double accents (e.g., a circumflex over a bar). Accents over characters can be eliminated by the use of such symbols as ', \*, and † set as superscripts.

If an accent or underscore has been used to designate a special typeface (e.g., boldface for vectors, script for transforms, sans serif for tensors), the type should be specified by a note in the margin.

If the argument of an exponential is complicated or lengthy, "exp" rather than  $e$  should be used. Awkward fractional composition can be avoided by the proper introduction of negative powers. In text, solidus fractions ( $l/r$ ) should be used, and enough enclosures should be included to avoid ambiguity. According to the accepted convention, parentheses, brackets, and braces are in the order { [ ( ) ] }. Displayed equations should be numbered consecutively throughout the paper; the number (in parentheses) should be to the right of the equation.

**Notation.** The notation is a list of symbols used in the text as an aid to the reader. It should be set up in this form:

- $c$  rate of soil accumulation, m/yr.
- $d$  median grain size of water-deposited material,  $\mu\text{m}$ .
- $D$  distance of the locus of points, m.
- $h$  elevation of the rock stream channel at a particular time  $t$ , meters above base level.
- $H_f$  maximum vertical displacement of the fault associated with an earthquake, m.
- $H_f'$  amount of vertical displacement of the mountain-bounding fault, m.
- $z$  vertical coordinate of the model grid system.
- $\beta$  parameter computed by  $\beta = b/\log_{10} e$ .
- $\gamma$  mean peak flow rate above base flow of stream,  $\text{m}^3\text{s}$ .

**References.** A complete and accurate reference list is of major importance. Omissions, discrepancies in the spelling of names, errors in titles, and incorrect dates make citations annoying, if not worthless, to the reader and cast doubt on the reliability of the author as well.

Only works cited in the text should be included in the reference list. References are cited in the text by the last name of the author and the year: [Jones, 1990]. If the author's name is part of the sentence, only the year is bracketed. Personal communications and unpublished data or reports are not included in the reference list; they should be shown parenthetically in text: (F. S. Jones, unpublished data, 1990).

References are arranged alphabetically by the last names of authors. Multiple entries for a single author are arranged chronologically. Two or more publications by the same author in the same year are distinguished by a, b, c after the year.

For laboratory, company, or government reports, information should be included on where the report can be obtained. For Ph.D.